ARTICLE IN PRESS

Available online at www.sciencedirect.com

ScienceDirect

Journal of Physics and Chemistry of Solids ▮ (▮▮▮▮) ▮▮▮–▮▮▮

JOURNAL OF PHYSICS AND CHEMISTRY OF SOLIDS

www.elsevier.com/locate/jpcs

Magnetic properties and EPR spectra of $[Cu(L\text{-arginine})_2](NO_3)_2 \cdot 3H_2O$

M.F. Gerard[a], C. Aiassa[a], N.M.C. Casado[a], R.C. Santana[b], M. Perec[c], R.E. Rapp[d], R. Calvo[a,*]

[a]*Departamento de Física, Facultad de Bioquímica y Ciencias Biológicas, Universidad Nacional del Litoral and INTEC (CONICET-UNL), Güemes 3450, 3000 Santa Fe, Argentina*

[b]*Instituto de Física, Universidade Federal de Goiás, Campus Samambaia, CP 131, 74001-970 Goiânia (GO), Brazil*

[c]*Departamento de Química Inorgánica, Analítica y Química Física, Facultad de Ciencias Exactas y Naturales, INQUIMAE, Universidad de Buenos Aires, Ciudad Universitaria, Pabellón II, 1428 Buenos Aires, Argentina*

[d]*Instituto de Física, Universidade Federal do Rio de Janeiro, CP 68528, 21941-972 Rio de Janeiro (RJ), Brazil*

Received 21 February 2007; received in revised form 17 March 2007; accepted 19 March 2007

Abstract

Magnetic and EPR data have been collected for complex $[Cu(L\text{-}Arg)_2](NO_3)_2 \cdot 3H_2O$ (Arg = arginine). Magnetic susceptibility χ in the temperature range 2–160 K, and a magnetization isotherm at $T = 2.29(1)$ K with magnetic fields between 0 and 9 T were measured. The observed variation of χT with T indicates predominant antiferromagnetic interactions between Cu(II) ions coupled in 1D chains along the $\boldsymbol{b}$ axis. Fitting a molecular field model to the susceptibility data allows to evaluate $g = 2.10(1)$ for the average g-factor and $J = -0.42(6)\,cm^{-1}$ for the nearest neighbor exchange coupling (defined as $\mathscr{H}_{ex} = -\sum J_{ij}\mathbf{S_i} \cdot \mathbf{S_j}$). This coupling is assigned to *syn–anti* equatorial–apical carboxylate bridges connecting Cu(II) ion neighbors at 5.682 Å, with a total bond length of 6.989 Å and is consistent with the magnetization isotherm results. It is discussed and compared with couplings observed in other compounds with similar exchange bridges. EPR spectra at 9.77 were obtained in powder samples and at 9.77 and at 34.1 GHz in the three orthogonal planes of single crystals. At both microwave frequencies, and for all magnetic field orientations a single signal arising from the collapse due to exchange interaction of resonances corresponding to two rotated Cu(II) sites is observed. From the EPR results the molecular g-tensors corresponding to the two copper sites in the unit cell were evaluated, allowing an estimated lower limit $|J| > 0.1\,cm^{-1}$ for the exchange interaction between Cu(II) neighbors, consistent with the magnetic measurements. The observed angular variation of the line width is attributed to dipolar coupling between Cu(II) ions in the lattice.

Keywords: D. Magnetic properties; D. Electron paramagnetic resonance

1. Introduction

Interest in the study of weak interactions in biomolecules and model systems is connected with their important role in supramolecular chemistry, which includes self-assembly processes [1,2], molecular recognition [3], magnetic exchange couplings [4], and electron transfer [5–7]. Paramagnetic metal–amino acid complexes are appropriate model systems for studying weak intermolecular interactions along amino acid bridging paths of biologically relevant molecules; exchange couplings between the metal ions connected by the paths provide information about their electronic structures [8]. Magnetic susceptibility and magnetization measurements are the standard thermodynamic tools for evaluating exchange interactions. EPR measurements in single crystal samples provide an appropriate technique to evaluate weak exchange interactions in the presence of stronger couplings supported by covalent bonds [9].

In the compound $[Cu(L\text{-}Arg)_2](NO_3)_2 \cdot 3H_2O$ reported by Masuda et al. [10] the central Cu(II) ion is in a CuO_2N_2 square-planar coordination with the N amino and O carboxylate atoms of two coordinated L-Arg molecules in a *cis* configuration. The crystal structure shows Cu(II) chains along the $\boldsymbol{b}$ axis coupled by equatorial–apical

*Corresponding author. Tel./fax: +54 342 460 8200.
E-mail address: calvo@fbcb.unl.edu.ar (R. Calvo).

0022-3697/$ - see front matter © 2007 Elsevier Ltd. All rights reserved.
doi:10.1016/j.jpcs.2007.03.032

carboxylate bridges, interconnected by a 3D network of H-bonds involving the guanidinium, nitrate, and water units. This differs from the compound $[Cu(L\text{-}Arg)_2](SO_4)\cdot 6H_2O$ [11], showing a set of right handed single helical chains running along the ***a*** axis. Cationic $[Cu(L\text{- or }D\text{-}Arg)_2]^{2+}$ with various dianions X^{2-} have been reported [2,10–14] and the suggestion was made that the strength and steric requirement for hydrogen bonds of the dianion are critical in determining the templating effect [15]. Here we report magnetic and single crystal EPR measurements in $[Cu(L\text{-}Arg)_2](NO_3)_2\cdot 3H_2O$ performed in order to study the electronic structure of the Cu(II) ions and the exchange interactions between Cu(II) neighbors connected by chemical paths containing carboxylate bridges. Considering the crystal structure, the magnetic susceptibility and magnetization data provides the magnitude of the exchange coupling J that is assigned to a syn–anti carboxylate group and it is compared with values reported for similar compounds. The EPR spectra are dominated by exchange narrowing and collapse processes and give information about the electronic structure of the metal ions.

2. Experimental

2.1. Sample preparation

$[Cu(L\text{-}Arg)_2](NO_3)_2\cdot 3H_2O$ was obtained as described by Masuda et al. [10] from L-arginine.HCl (0.84 g, 4.0 mmol) and $Cu(NO_3)_2$ (0.48 g, 2.0 mmol) in water. The amino acid and the metal salt were obtained from Sigma and used without further purification. The resulting solution, adjusted to pH = 6.5 with NaOH 0.1 N, was filtered through a cellulose nitrate membrane and left to evaporate at room temperature. Blue rectangular single crystal plates elongated along the ***b*** axis grew after a few days. Elemental analysis was performed on a Carlo Erba 1108 analyzer and the IR spectrum was recorded on a FT-IR Nicolet 510 P spectrophotometer (KBr pellet). The powder X-ray diffraction pattern (Cu Kα) obtained on a Siemens D5000 diffractometer agrees satisfactorily with that calculated with the program Mercury [16] using the X-ray data of a single crystal reported by Masuda et al. [10]. The EPR spectrum at 9.77 GHz of the same powder material used in the X-ray measurements was obtained and used as a fingerprint of the material for subsequent synthesis procedures.

2.2. Magnetic measurements

The magnetic susceptibility of a gelatin capsule sample holder with 119 mg of powdered $[Cu(L\text{-}Arg)_2](NO_3)_2\cdot 3H_2O$ was measured at temperatures T between 2 and 160 K with applied magnetic field $B_0=\mu_o H=0.2$ T (μ_o is the vacuum permeability) with a PPMS magnetometer (Quantum Design, Inc.). *ac* susceptibility with an excitation field of 0.1 mT at 1 kHz was also measured with equal results within the accuracy of the measurements. A magnetization isotherm at $T=2.29(1)$ K was measured with B_0 between 0 and 9 T. A diamagnetic contribution $\chi_d=-0.26\times10^{-3}\,cm^3/mol$ calculated from the chemical formula, was subtracted from the data.

2.3. EPR measurements

The EPR measurements were performed in ER−200 and ESP−300 Bruker spectrometers working at 9.77 and at 34.1 GHz, respectively, with standard Bruker cavities operating with 100 kHz magnetic field modulation, and rotating magnets. The magnetic field B_0 was calibrated using diphenylpicrylhydrazyl (DPPH) positioned close to the sample as field marker ($g=2.0036$). EPR spectra ($d\chi''/dB_0$) from powdered material and from oriented single crystals were collected digitally at room temperature. The orientation of the samples for the single crystal EPR measurements were attained by gluing a *bc* growth face to a cubic piece of KCl single crystal holder obtained by cleavage, with the ***b*** axis along a side of the cube. This holder defines a set of orthogonal axes ***x***, ***y***, ***z*** along the $\boldsymbol{a}^*=\boldsymbol{b}\times\boldsymbol{c}$, ***b*** and ***c*** crystal axes of the sample. The single crystal spectra were collected at 5° intervals in the orthogonal planes a^*b, a^*c and *bc* in a range of 180°. A single resonance line without hyperfine splitting was observed for all orientations of $\boldsymbol{B}_0$ in these three planes. The position and peak-to-peak line width ΔB_{pp} of this resonance were obtained by least squares fits of the field derivative of a Lorentzian line shape to the observed signal. Good agreement was obtained between the observed spectra and these fits, which provide the *g*-factors and line widths.

3. Experimental results and analysis

3.1. Magnetic measurements

Fig. 1 displays the *ac* magnetic susceptibility χ observed at 1 kHz with an excitation field of 0.1 mT as χT *vs.* T. At high temperatures $\chi T=0.416\,cm^3\,K/mol$, and $\mu_{eff}/\mu_B=(3k_B/N_{Av})^{1/2}(\chi T)^{1/2}/\mu_B=[g^2S(S+1)]^{1/2}=1.824$, indicating $g=2.10$ for the average *g*-factor of the $S=\frac{1}{2}$ Cu(II) ions. The effective magnetic moment χT decreases rapidly below 10 K indicating predominant antiferromagnetic coupling between Cu(II) ions. Fig. 2 displays the magnetization isotherm measured at $T=2.29(1)$ K. At the highest field, 9 T, the magnetization is close to saturation.

We define the exchange interactions between two spins $\boldsymbol{S_1}$ and $\boldsymbol{S_2}$ by [8]:

$$\mathscr{H}_{ex}=-J\boldsymbol{S_1}\cdot\boldsymbol{S_2} \quad (1)$$

The exchange coupling J between nearest neighbor Cu(II) ions was evaluated from the data in Fig. 1 using a

Please cite this article as: M.F. Gerard, et al., J. Phys. Chem. Solids (2007), doi:10.1016/j.jpcs.2007.03.032

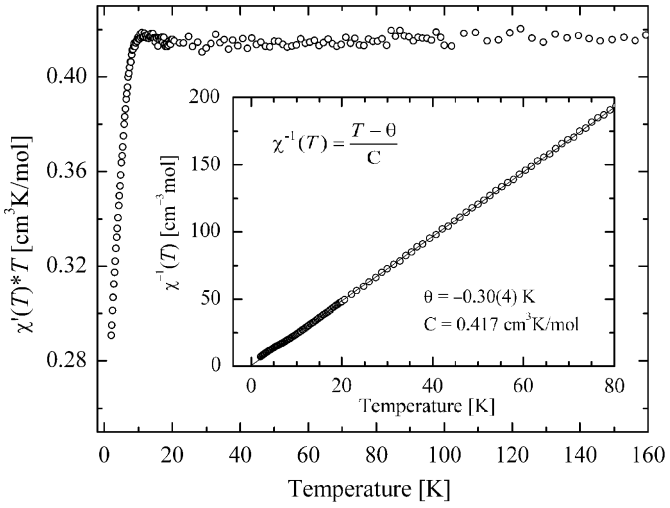

Fig. 1. *ac* magnetic susceptibility of $[Cu(L\text{-}Arg)_2](NO_3)_2 \cdot 3H_2O$ observed at 1 kHz, with an excitation field of 0.1 mT. The diamagnetic contribution has been subtracted. These results are equal to the *dc* susceptibility observed at 0.2 T. The inset shows a plot of the observed values of $\chi^{-1}(T)$ vs. T and the corresponding fit to a Curie–Weiss law, giving the parameters displayed in the figure.

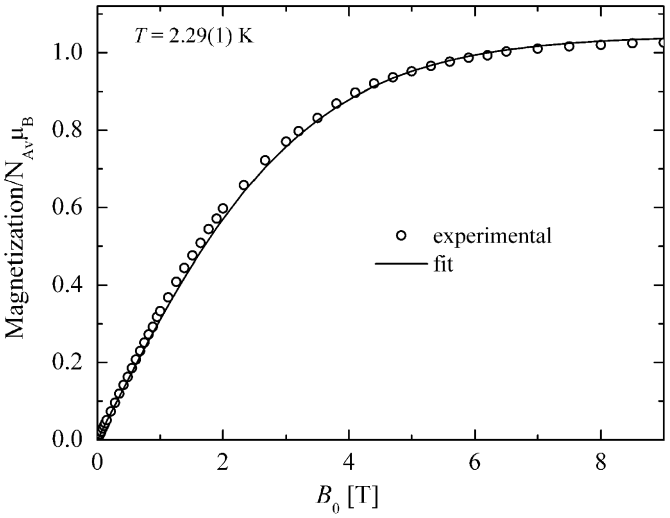

Fig. 2. Molecular magnetization of $[Cu(L\text{-}Arg)_2](NO_3)_2 \cdot 3H_2O$ between 0 and 9 T measured at $T = 2.29(1)$ K. The diamagnetic contribution has been subtracted. The solid line is obtained with the parameters calculated from the susceptibility data.

molecular field approximation [8,17]:

$$\chi(T) = \frac{N_{Av} g^2 \mu_B^2}{4k_B(T-\Theta)}, \quad (2)$$

where μ_B is the Bohr magneton,

$$\Theta = \frac{zJS(S+1)}{3k_B}, \quad (3)$$

N_{Av} the Avogadro's number and zJ is the molecular field parameter. Since each Cu(II) ion is connected to $z = 2$ copper neighbors along a spin chain we obtained $\Theta = -0.30(4)$ K and, using Eq. (3), $J = -0.42(6)\,cm^{-1}$ from the susceptibility data in Fig. 1. The solid line for the isothermal magnetization in Fig. 2, obtained with the same parameters, agrees with the observed magnetization within 1%. The deviation could indicate a weaker ferromagnetic interaction between chains, but we were not able to evaluate it.

An alternative procedure to evaluate J from magnetic data in materials with Heisenberg coupling along one dimension is that introduced by Bonner and Fisher [18] which allows to calculate susceptibility and specific heat of antiferromagnetic spin chains with a maximum value at $k_BT \sim J$ and a very characteristic T dependence in this range and below. However, we observed that when temperatures are considerably higher, the latter method gives similar results and does not offer advantages compared with the molecular field approximation used in this work.

3.2. EPR measurements

3.2.1. Crystal and molecular g-tensors

Fig. 3 displays the EPR spectrum of a powder sample of $[Cu(L\text{-}Arg)_2](NO_3)_2 \cdot 3H_2O$. We fitted this spectrum using the EasySpin package [18] and optimization routines provided by Matlab, with a model consisting of $\frac{1}{2}$ spins with anisotropic g-tensor and intrinsic line width displaying a tensorial angular dependence, with the same principal axes as the g-tensor. The calculated principal values of the g-tensor and line width are included in Table 1. The dotted line in Fig. 3 is the spectrum simulated with these values. The small differences between measured and simulated spectra are attributed to the deviation of the angular variation of the line width from the assumed second degree tensorial angular variation (see later in the single crystal results).

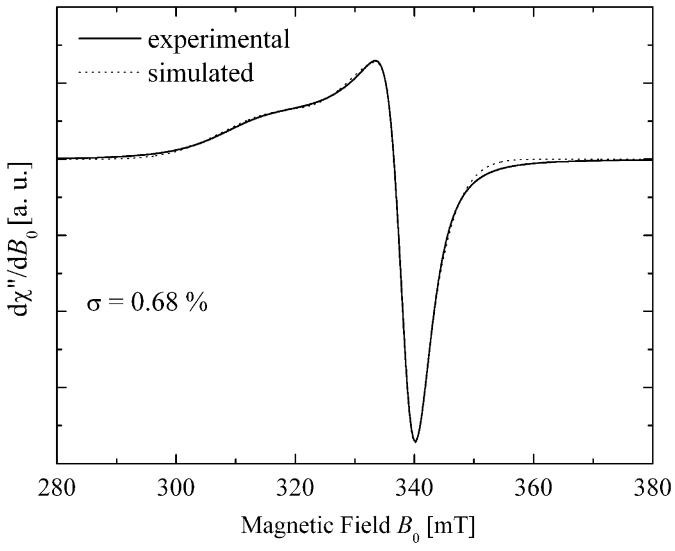

Fig. 3. EPR spectrum of a powder sample of $[Cu(L\text{-}Arg)_2](NO_3)_2 \cdot 3H_2O$. Solid line is experimental result. Dotted line is the simulation with the parameters given in Table 1 obtained as described in the text. σ is the standard deviation of the residues between experimental and simulated spectra.

Please cite this article as: M.F. Gerard, et al., J. Phys. Chem. Solids (2007), doi:10.1016/j.jpcs.2007.03.032

Table 1
(*a*) Eigenvalues g_1, g_2 and g_3 of the $\boldsymbol{g}$-tensor and the line width obtained from a fit of the powder EPR spectrum of Fig. 3 (see text); (*b*) components of the crystal $\boldsymbol{g^2}$ tensor obtained by least squares fits of the function $g^2(\theta,\phi) = (\boldsymbol{h.g.g.h})$ to the experimental data taken at 9.77 GHz (not shown) and at 34.1 GHz (displayed in Fig. 4): $(g^2)_1$, $(g^2)_2$, $(g^2)_3$ and $\boldsymbol{a_1}$, $\boldsymbol{a_2}$, $\boldsymbol{a_3}$ are the eigenvalues and eigenvectors of this tensor and $g_\perp$ and $g_{//}$ were calculated for the molecular $\boldsymbol{g}$ tensor of the Cu(II) ions assuming axial symmetry

(*a*) Parameters obtained from the powder spectrum at 9.77 GHz			
g_1	2.062	ΔB_1	14 mT
g_2	2.063	ΔB_2	3.9 mT
g_3	2.222	ΔB_3	20 mT
(*b*) Parameters obtained from the single crystal results			
	$\nu = 9.77$ GHz		$\nu = 34.1$ GHz
$(g^2)_{xx}$	4.2305(8)		4.2203(3)
$(g^2)_{yy}$	4.9581(8)		4.9449(3)
$(g^2)_{zz}$	4.2559(8)		4.2582(3)
$(g^2)_{xy}$	0.000(1)		0.000(1)
$(g^2)_{zx}$	0.021(1)		0.0274(4)
$(g^2)_{zy}$	0.000(1)		0.000(1)
$(g^2)_1$	4.218(1)		4.2059(4)
$(g^2)_2$	4.268(1)		4.2726(4)
$(g^2)_3$	4.958(1)		4.9449(3)
$\boldsymbol{a_1}$	[0.870(7), 0.000(7), 0.49(1)]		[0.885(2), 0.000(2), 0.465(4)]
$\boldsymbol{a_2}$	[0.49(1), 0.000(8), −0.870(7)]		[0.465(4), 0.000(4), −0.885(2)]
$\boldsymbol{a_3}$	[0.000(1), 1, 0.005(5)]		[0.000(4), 1, 0.000(5)]
$g_{//}$	2.238		2.239
$g_\perp$	2.0538		2.0509
2α	29.1°		33.4°
θ_m	102.6°		104.8°
ϕ_m	82.7°		82.0°

Notes: The largest eigenvalue $(g^2)_3$ corresponds to the direction of the crystal $\boldsymbol{b}$-axis. We include the angles 2α between the normals $\mathbf{n}_A$ and $\mathbf{n}_B$ to the planes of ligands to Cu(II) ions in lattice sites A and B, and of (θ_m, ϕ_m) for the orientation of the direction of $g_{//}$ for site A in the lattice, calculated from the EPR data.

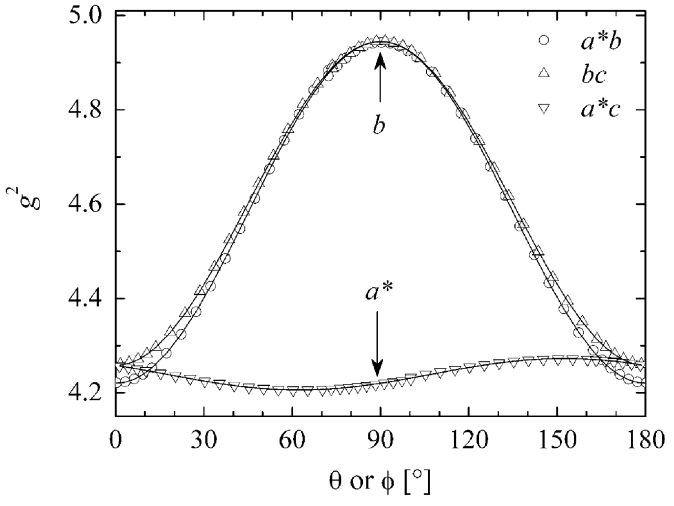

Fig. 4. Angular variation of $g^2(\theta,\phi)$ at 34.1 GHz for the magnetic field applied in the a^*b, a^*c and bc crystalline planes of $[Cu(L\text{-}Arg)_2](NO_3)_2 \cdot 3H_2O$. The solid lines are calculated with the values of the components of the g^2 tensor at 34.1 GHz included in Table 1 The results obtained at 9.77 GHz agree within the experimental uncertainties.

Fig. 4 displays the observed angular variation of g^2 in the three studied planes at 34.1 GHz. Similar data at 9.77 GHz (not shown) are less accurate, but equal within uncertainties. The angular variation of the position of the observed single collective resonance is described by the spin Hamiltonian [19]:

$$\mathscr{H}_z = \mu_B \mathbf{S} \cdot \boldsymbol{g} \cdot \boldsymbol{B_0}, \tag{4}$$

where $\mathbf{S}$ is the effective spin operator ($S = \frac{1}{2}$), $\boldsymbol{B_0} = B_0\boldsymbol{h}$ is the magnetic field applied along $\boldsymbol{h} = \boldsymbol{B_0}/|\boldsymbol{B_0}|$ and $\boldsymbol{g}$ is the crystal $\boldsymbol{g}$-tensor, corresponding to the coupled spin system. The single resonance is assigned to the collapse of those corresponding to coppers in sites A and B, thus the crystal g-tensor $\boldsymbol{g}$ is interpreted as the average of the molecular $\boldsymbol{g_i}$-tensors (i = A, B) corresponding to the two rotated Cu(II) sites in the unit cell [9]:

$$\boldsymbol{g} = \tfrac{1}{2}(\boldsymbol{g_A} + \boldsymbol{g_B}). \tag{5}$$

The components of the squared crystalline $\boldsymbol{g}$-tensor in the $xyz \equiv a^*bc$ system of axes, were obtained by least squares fitting to the observed values in Fig. 4 of the function:

$$\begin{aligned} g^2(\theta,\phi) = \boldsymbol{h}\cdot\boldsymbol{g}\cdot\boldsymbol{g}\cdot\boldsymbol{h} = {} & (g^2)_{xx}\sin^2\theta\cos^2\phi \\ & + (g^2)_{yy}\sin^2\theta\sin^2\phi + (g^2)_{zz}\cos^2\theta \\ & + 2(g^2)_{xy}\sin^2\theta\sin\phi\cos\phi \\ & + 2(g^2)_{xz}\sin\theta\cos\theta\cos\phi \\ & + 2(g^2)_{yz}\sin\theta\cos\theta\sin\phi. \end{aligned} \tag{6}$$

The tensorial components of the $\boldsymbol{g^2}$ crystalline tensor are given in Table 1 together with their eigenvalues and eigenvectors. The solid lines (Fig. 4) calculated with Eq. (6), and the components of the $\boldsymbol{g^2}$ tensor given in Table 1, are in good agreement with the data. Using Eq. (5) and a procedure described previously [20–22], the molecular $\boldsymbol{g_i}$-tensors (i = A,B) of the individual Cu(II) ions in $[Cu(L\text{-}Arg)_2](NO_3)_2 \cdot 3H_2O$ were evaluated assuming axial symmetry, with θ_m and ϕ_m as the polar and azimuthal angles corresponding to the direction along which $g_\parallel$ would be measured for magnetically isolated Cu(II) ion in crystal site A. With this assumption the EPR results give the molecular values $g_\parallel$, $g_\perp$, θ_m, ϕ_m and the angle 2α between the parallel directions corresponding to Cu(II) sites A and B [22] included in Table 1. The values of $g_\parallel$ and $g_\perp$ are consistent with a $d(x^2-y^2)$ ground state orbital of the Cu(II) ions [23] in $[Cu(L\text{-}Arg)_2](NO_3)_2 \cdot 3H_2O$, as observed in similar compounds [22,24–28]. The values of the angles θ_m, ϕ_m and the angle 2α evaluated from the EPR data (Table 1) are in a good agreement with the values $\theta_c = 104.2°$, $\phi_c = 84.1°$ and $2\alpha_c = 30.7°$ calculated from the crystal structure information [10] for the normal to the plane of equatorial ligands to copper. The observed collapse of the EPR lines of the Cu(II) sites for all magnetic field directions at 34.1 GHz points out [9] a lower limit $|J| \geqslant 1/2(g_A - g_B)\mu_B B_0 \approx 0.1\,\mathrm{cm}^{-1}$ for the exchange

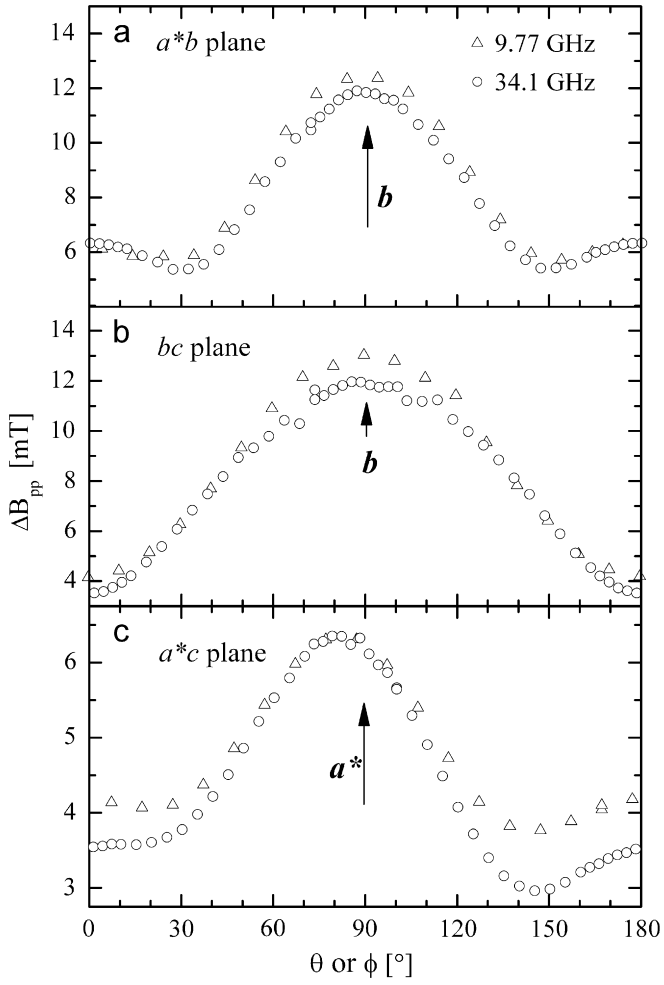

Fig. 5. Angular variation of the peak-to-peak line width ΔB_{pp} measured at 9.77 and 34.1 GHz in the a^*b plane (a), bc plane (b), and a^*c plane (c) of a $[Cu(L\text{-}Arg)_2](NO_3)_2 \cdot 3H_2O$ single crystal.

interaction between neighboring Cu(II) ions of both types A and B.

3.2.2. The EPR line width

The angular variations of the peak-to-peak line width $\Delta B_{pp}(\theta,\phi)$ observed at 9.77 and 34.1 GHz in the a^*b, a^*c and bc planes are displayed in Figs. 5a–c. Several contributions to the EPR broadening arising from dipolar interactions, incomplete collapse of the signals of the two sites, and of the hyperfine splitting, have been identified and reported in Cu(II) amino acid complexes [24,25]. In the present case the line width observed in the three crystalline planes is nearly frequency independent, indicating that the residual Zeeman interaction does not contribute [9,25,29]. Thus, the observed width is interpreted as a consequence of the magnetic dipolar interactions between copper ions, narrowed by the exchange interactions. It is observed in Figs. 5a–c that the line width does not follow exactly a second-order tensorial angular dependence. This explains the small deviation of the simulation of the powder spectrum (that assumes tensorial dependence) from the experimental result.

4. Discussions

The value of J is the sum of positive (ferromagnetic) and negative (antiferromagnetic) contributions. As reported by Colacio and collaborators [30], when Cu(II) ions are connected by *syn–anti* equatorial–apical carboxylate bridges, the two contributions have similar magnitudes and the exchange coupling is small and may be ferromagnetic or antiferromagnetic. The magnitude of the magnetic interactions between copper ions may be discussed on the basis of the structural features of the bridging network, together with the nature of the orbitals involved in the exchange interactions. Thus, using the X-ray structure reported by Masuda et al. [10] we display in Fig. 6a a central A molecule together with a neighbor B type Cu(II) molecule, emphasizing the bridging system making the connection between these CuA–CuB neighbor ions at 5.682 Å. There is a *syn–anti* equatorial–apical carboxylate bridge $–Cu_A–O3–C7–O4–Cu_B–$ with three diamagnetic atoms and total bond length of 6.989 Å. In parallel is the bridge $–Cu_A–N5–C8–C7–O4–Cu_B–$, with four diamagnetic atoms and a total length of 8.717 Å. This bridging system gives rise to Cu(II) chains along the ***b*** axis (see Fig. 6b). A Cu(II) ion type A is also connected to two Cu(II) type B at 9.367 Å in a neighbor chain (see Fig. 6c). These shortest interchain chemical bridges, which are sketched in Fig. 6c, contain eight diamagnetic atoms including a weak hydrogen bond and have a total length of 13.868 Å. We assume that they support the strongest interchain contributions to the exchange interaction network. Other interchain bridges, also sketched in Fig. 6c, are even longer. Thus, the *syn–anti* carboxylate bridge O3–C7–O4 (Figs. 6a,b) supports the strongest exchange coupling between copper ions.

Levstein and Calvo [29] proposed that the magnitude $|J|$ of the exchange coupling is mainly dependent of the length of the weakest segment of the path, between the Cu(II) ion and its apical oxygen ligand. Fig. 7 shows a linear dependence for the previously reported copper complexes with L-methionine (L-Met), L-leucine (L-Leu) and L-phenylalanine (L-Phe) [29], together with the new data for $[Cu(L\text{-}Arg)_2](NO_3)_2 \cdot 3H_2O$, suggesting a common behavior in a group of compounds with similar exchange paths. The quality of the agreement may not be so good if paths with a wider variety of angular parameters are considered [31]. The interactions between Cu(II) ions in neighbor chains supported by the charged groups of arginine and the NO_3^- ions are very weak and, correspondingly, would be the exchange interactions.

In conclusion, this work reports a magnetic and single crystal EPR study of electronic properties and magneto-structural correlations in $[Cu(L\text{-}Arg)_2](NO_3)_2 \cdot 3H_2O$. The magnetic study provides the magnitude of the exchange interaction between nearest neighbor Cu(II) ions that is

Please cite this article as: M.F. Gerard, et al., J. Phys. Chem. Solids (2007), doi:10.1016/j.jpcs.2007.03.032

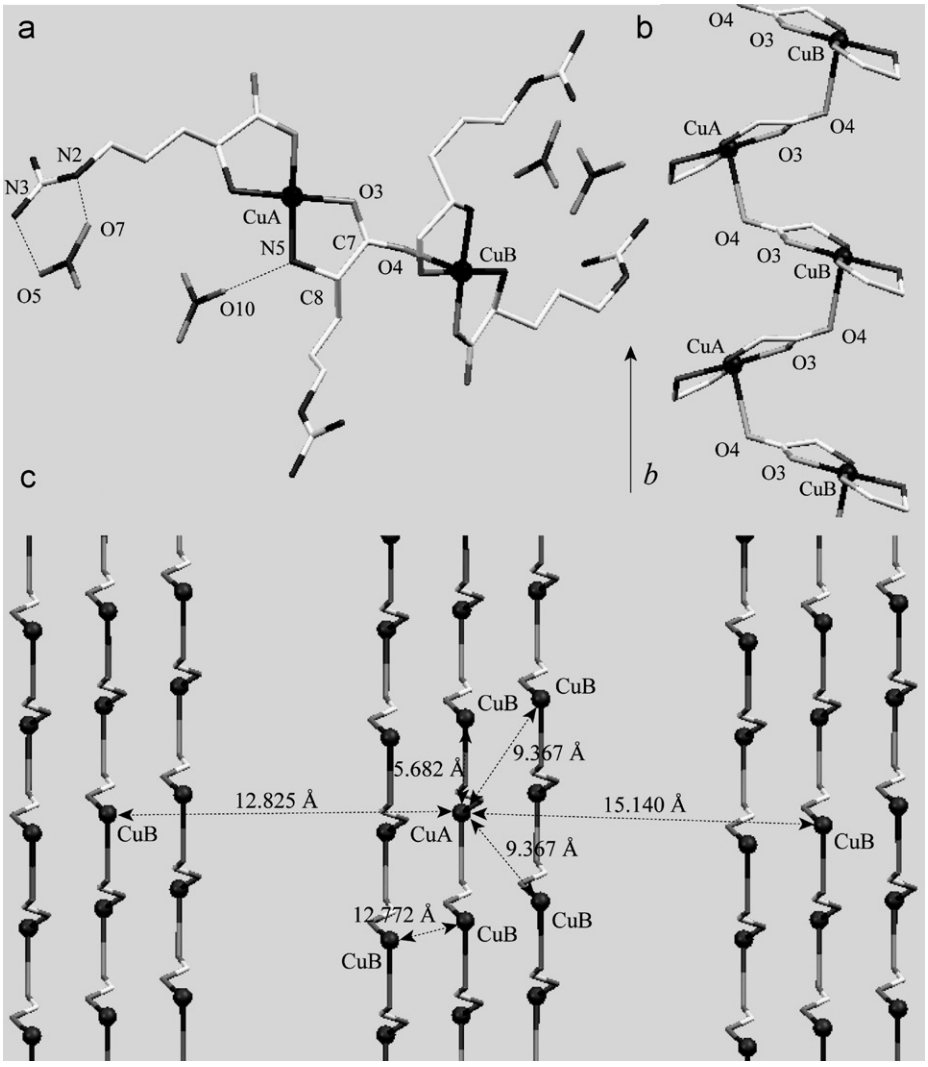

Fig. 6. Molecular structure of $[Cu(L\text{-}Arg)_2](NO_3)_2 \cdot 3H_2O$ (values taken from Ref. [10]). (a) Two neighbor rotated molecules connected by a carboxylate bridge. For clarity water molecules are not included. (b) Copper chain along the ***b***-axis. (c) Distances between copper ions for intra and interchain connections. The copper chains are those displayed in (b).

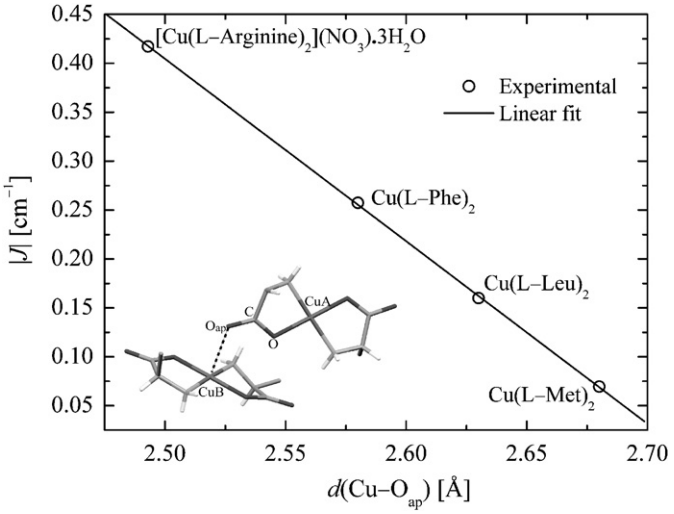

Fig. 7. Plot of J values of four Cu(II) amino acid complexes with similar bridges vs. $d(Cu–O_{ap})$. The equatorial–apical bridge is shown in the inset (see also Fig. 6a).

assigned to a *syn–anti* equatorial–apical carboxylate bridge in the structure. These results compare well with measurements in compounds with similar bridges and provide grounds for future theoretical work. From the single crystal EPR data we evaluate the principal values and directions of the crystal and molecular g-tensors of the Cu(II) ion, that provide information about the electronic structure of the individual copper ions.

Acknowledgments

We thank to the Spanish Research Council (CSIC) for providing us with free-of-charge licenses to the Cambridge Structural Database [32,33]. The work in Argentina was supported by grants CAI+D–UNL, PIP 5274 and ANPCyT PICT 06–13782. The work in Brazil was supported by CNPq, FAPERJ and CAPES. MP and RC are members of CONICET.

References

[1] N. Ohata, H. Masuda, O. Yamauchi, Angew. Chem. Int. Ed. Engl. 35 (1996) 531.
[2] O. Yamauchi, A. Odani, M. Takani, J. Chem. Soc, Dalton. Trans. (2002) 3411.
[3] S.J. Lippard, J.M. Berg, Principles of Bioinorganic Chemistry, University Science Books, Mill Valley CA, 1994.
[4] E.I. Solomon, D.E. Wilcox, in: R.D. Willet, D. Gatteschi, O. Kahn (Eds.), Magneto Structural Correlations in Exchange Coupled Systems, Reidel, Dordrecht, 1985, p. 463.
[5] E.L. Bominaar, C. Achim, S.A. Borshch, J.J. Girerd, E. Münck, Inorg. Chem. 36 (1997) 3689.
[6] P. Chen, E.I. Solomon, Proc. Natl. Acad. Sci. USA 101 (2004) 13105.
[7] E.A. Weiss, M.R. Wasielewski, M.A. Ratner, J. Chem. Phys. 123 (2005) 064504.
[8] O. Kahn, Molecular Magnetism, VCH, New York, 1993.
[9] R. Calvo, Appl. Magn. Reson. 31 (2007) 271.
[10] H. Masuda, A. Odani, T. Yamazaki, T. Yahima, O. Yamauchi, Inorg. Chem. 32 (1993) 1111.
[11] N. Ohata, H. Masuda, O. Yamauchi, Inorg. Chim. Acta 300–302 (2000) 749.
[12] M.T.L.S. Duarte, M.A.A.F.D. Carrondo, M.L.S. Goncalves, M.B. Hursthouse, N.P.C. Walker, H.M. Dawes, Inorg. Chim. Acta 124 (1986) 41.
[13] I. Viera, M.H. Torre, O.E. Piro, E.E. Castellano, E.J. Baran, J. Inorg. Biochem. 99 (2005) 1250.
[14] N. Ohata, H. Masuda, O. Yamauchi, Inorg. Chim. Acta 286 (1999) 37.
[15] R. Vilar, Angew. Chem. Int. Ed. 42 (2003) 1460.
[16] I.J. Bruno, J.C. Cole, P.R. Edington, M. Kessler, C.F. Macrae, P. McCabe, J. Pearson, R. Taylor, Acta Crystallogr. B 58 (2002) 389.
[17] C.J. O'Connor, Prog. Inorg. Chem. 29 (1982) 203.
[18] S. Stoll, A. Schweiger, J. Magn. Reson. 178 (2006) 42.
[19] A. Abragam, B. Bleaney, Electron Paramagnetic Resonance of Transition Metal Ions, Oxford, UK, 1971.
[20] H. Abe, K. Ono, J. Phys. Soc. Jpn. 11 (1956) 947.
[21] D.E. Billing, B.J. Hathaway, J. Chem. Phys. 50 (1969) 1476.
[22] R. Calvo, M. Mesa, Phys. Rev. B 28 (1983) 1244.
[23] H.J. Zweiger, G.W. Pratt, Magnetic Interactions in Solids, Oxford University Press, London, 1973.
[24] A.M. Gennaro, P.R. Levstein, C.A. Steren, R. Calvo, Chem. Phys. 111 (1987) 431.
[25] P.R. Levstein, C.A. Steren, A.M. Gennaro, R. Calvo, Chem. Phys. 120 (1988) 449.
[26] A.J. Costa-Filho, O.R. Nascimento, L. Ghivelder, R. Calvo, J. Phys. Chem. B 105 (2001) 5039.
[27] A.J. Costa Filho, O.R. Nascimento, R. Calvo, J. Phys. Chem. B 108 (2004) 9549.
[28] E.D. Vieira, N.M.C. Casado, G. Facchin, M.H. Torre, O.R. Nascimento, A.J. Costa-Filho, R. Calvo, Inorg. Chem. 45 (2006) 2942.
[29] P.R. Levstein, R. Calvo, Inorg. Chem. 29 (1990) 1581.
[30] E. Colacio, M. Ghazi, R. Kivekäs, J.M. Moreno, Inorg. Chem. 39 (2000) 2882 and references therein.
[31] J.M. Schveigkardt, A.C. Rizzi, O.E. Piro, E.E. Castellano, R.C. Santana, R. Calvo, C.D. Brondino, Eur. J. Inorg. Chem. 2002 (2002) 2913.
[32] F.H. Allen, Acta Crystallogr. B 58 (2002) 380.
[33] A.G. Orpen, Acta Crystallogr. B 58 (2002) 398.

Please cite this article as: M.F. Gerard, et al., J. Phys. Chem. Solids (2007), doi:10.1016/j.jpcs.2007.03.032